ap

Asian Journal of Physics
Vol. 26, No 1 (2017) 09-19
Available on: www.asianjournalofphysics.in

A measurement of the strongly forbidden $6S_{1/2} \leftrightarrow 5D_{3/2}$ Magnetic dipole transition moment in Ba^+

Spencer R Williams, Anupriya Jayakumar, Matthew R Hoffman, Boris B Blinov,* and E N Fortson
Department of Physics, University of Washington, Seattle, Washington, 98195, USA

We report the results from our first-generation experiment to measure the magnetic-dipole transition moment (M1) between the $6S_{1/2}$ and $5D_{3/2}$ manifolds in Ba^+. Knowledge of M1 is crucial for the proposed parity-nonconservation experiment in the ion [1], where M1 will be a leading source of systematic error. To date, no measurement of M1 has been made in Ba^+, and moreover, the sensitivity of the moment to electron-electron correlations has prevented accurate theoretical predictions. A precise measurement may help to resolve the theoretical discrepancies while providing essential information for planning a future PNC measurement in Ba^+. We demonstrate our technique for measuring M1 - including a method for calibrating for stress-induced birefringence introduced by the scientific apparatus - and report our first measurement yielding $M1 = 93 + 38 - 40 \times 10^{-5}$ μB.

Key words: Barium, Spectroscopy, Forbidden transitions, Parity Non-Conservation

1 Introduction

Atomic parity nonconservation (APNC) measurements continue to be of interest for the breadth of physics they may illuminate [2-5]. Presently, several experiments are underway to search for parity violating effects in atoms and molecules [6-11]. One path being pursued for next-generation APNC studies is to investigate the effect in single trapped atomic ions, following the approach proposed in [1], for which Ba^+ is exemplar. In that system, the largest observable consequence of APNC is the emergence of a small electric-dipole transition moment ($E1_{APNC}$) between the ion's $6S_{1/2}$ ground states and its low-laying metastable $5D_{3/2}$ states. In addition to $E1_{APNC}$, there is also an electric-quadrupole transition moment (E2) and magnetic-dipole transition moment (M1) connecting those states. To measure $E1_{APNC}$, the size of these other, much larger, transition moments must be known. Some work has been undertaken that placed E2 at 12.7 $(a_0 / \lambda)\, e a_0$ [12, 13], where e is the electron charge, a_0 is the Bohr radius, however, to the best of our knowledge, no measurement of M1 has been performed and there is significant disagreement between the numerical studies [12, 14, 15]. In this paper we present the results of our first measurement of M1.

2 Background

The principal challenge in measuring the $6S_{1/2} \leftrightarrow 5D_{3/2}$ M1 transition matrix element in Ba^+ is that its effect must be isolated from the much larger E2 coupling.

These two transition moments explicitly are,

$$E2 = \langle 6S_{1/2} || \widehat{E2} \; 5D_{3/2} \rangle \tag{1a}$$

$$M1 = \langle 6S_{1/2} || \widehat{M1} \; 5D_{3/2} \rangle \tag{1b}$$

where the operators $\widehat{E2}$ and $\widehat{M1}$ are defined as,

Corresponding author
e-mail: blinov@uw.edu (Boris B Blinov)

$$\widehat{\mathrm{E2}} = -\frac{1}{6}\,\widehat{\mathrm{Q}}_{i,j}\,\frac{\partial E_i}{\partial X_j} \tag{2a}$$

$$\widehat{\mathrm{M1}} = -\vec{\widehat{M}}\,.\,\vec{B} \tag{2b}$$

where $\widehat{\mathrm{Q}}_{i,j}$ and $\vec{\widehat{M}}$ are the (electric) quadrupole and (magnetic) dipole operators, respectively, and $\vec{E}$ and $\vec{B}$ are the applied electric and magnetic fields. The matrix element E2 is known, to the 1% level, to be 12.7 (a_0/λ) ea_0 [12, 13]. However, to the best of our knowledge, only three calculations of M1 have been performed which, in terms of the Bohr magneton μ_B, have given;

$$\mathrm{M1} = \begin{cases} 80 \times 10^{-5}\ \mathrm{1/B}\ [12] \\ 22 \times 10^{-5}\ \mathrm{1/B}\ [14] \\ 17 \times 10^{-5}\ \mathrm{1/B}\ [15] \end{cases} \tag{3}$$

The large range of values obtained in those studies has been attributed to those author's estimations of electron-electron correlation effects in the atom [15]. That discrepancy withstanding, there is agreement on its order of magnitude, which places M1/E2 at $\sim 10^{-3}$.

For any of the $6S_{1/2} \leftrightarrow 5D_{3/2}$ transitions in Ba^+, which have their resonances nominally at 2.051 μm, the total Rabi frequency ignoring APNC, Ω, is,

$$\Omega = |\Omega_{\mathrm{E2}} + \Omega_{\mathrm{M1}}| \tag{4}$$

We seek M1 within the Δm $6S_{1/2}$(m = –1/2) and $5D_{3/2}$(m transition between the –1/2) states, for which, in terms of the reduced transition matrix elements of Eq (1), the E2 and M1 contributions are,

$$\Omega^{(0)}_{\mathrm{E2}} = \frac{ik}{4\hbar}\sqrt{\frac{1}{10}}\,\mathrm{M2}\,\sin(2\theta)\,\mathrm{E}_{\parallel} \tag{5a}$$

$$\Omega^{(0)}_{\mathrm{E1}} = -\frac{1}{\hbar}\sqrt{\frac{1}{6}}\,\mathrm{M1}\,\sin(\theta)\,\mathrm{B}_{\parallel}, \tag{5b}$$

where the superscript identifies the change in the magnetic quantum number for the transition, i is the complex unit, and k is the driving field's wave-vector. The angle θ is that between the 2.051 μm beam and the ion's quantization axis. The $\parallel$ and $\perp$ subscripts on the driving field components describe their orientation relative to the plane spanned by those vectors, with $\parallel$ being the in-plane component and $\perp$ the normal component. It follows that by driving the Δm = 0 transition with a perfectly linear polarized field, the electric-quadrupole coupling can be turned off by rotating the 2.051 μm beam's polarization to an orientation where its electric field is perpendicular to the quantization axis.

The alignment angle θ cannot be distinguished well within the Δm = 0 transition since, independent of the ratio of M1 to E2, it also affects the relative size of the two Rabi frequency contributions. Its effect, however, is clearly discernible within the Δm = ±2 transitions due to the strong coupling to both the parallel ($\mathrm{E}_{\parallel}$) and perpendicular ($\mathrm{E}_{\perp}$) components of the driving electric field. Generically, the Rabi frequency for Δm = ± 2 is:

$$\Omega^{(\pm 2)} = \frac{30}{2\sqrt{30\hbar}}\,E2\,\left|\frac{1}{2}\sin(2\theta)\mathrm{E}_{\parallel} + i\,\sin(\theta)\,\mathrm{E}_{\perp}\right| \tag{6}$$

Observe also that Eq (5) and Eq (6) hold true regardless of the 2.051 μm polarization state. Because the M1 coupling is so small relative to the E2 coupling, distortions to the driving field polarization state are a leading systematic concern. In practice, we have found that the small amounts of ellipticity induced from birefringence of the optical viewport leading into the trapping apparatus are significant and must be accounted for in the analysis.

3 Apparatus Summary

Single ions were trapped inside a linear Paul trap, described in [9], with ~440 kHz axial and ~1 MHz radial trapping frequencies. Micromotion was compensated for by means of a disk electrode beneath the trap and a rod electrode parallel to the trap axis. A small hole bored through the center of the disk electrode allowed neutral barium flux to reach the trap from an oven below. The trap was loaded by a two step photo-ionization process [16]. The neutral atoms were first excited along their narrow inter-combination line at 791 nm connecting the ground states to the 6S6P $^3P_0$ excited states. This transition is sufficiently narrow to allow for isotope selective loading. From the excited level the atoms were ionized with a 337 nm photon from a N_2 laser.

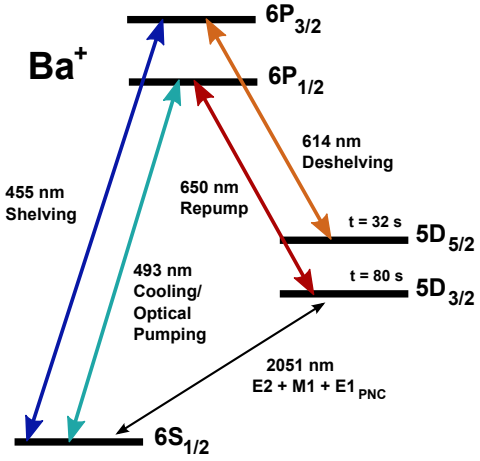

Fig 1. A diagram of the valence structure of Ba^+ including the various transitions used in the course of this experiment.

The single trapped ions were cooled to ~2 mK by Doppler cooling along the ion's $6S_{1/2} \leftrightarrow 6P_{1/2}$ transition at 493 nm. The ion's Λ-structure, represented in Fig 1 alongwith the transitions relevant to this study, necessitates a second "repump" beam at 650 nm. The primary cooling beam was produced by frequency-doubling an external cavity diode laser (ECDL) operating at 986 nm. A small percentage of the main cooling beam was picked off and circularly polarized for optical pumping. The 650 nm beam was produced by a commercial 650 nm ECDL. Both beams were stabilized against highly isolated optical resonators.

State read-out along the $6S_{1/2} \leftrightarrow 5D_{3/2}$ transitions was accomplished using an electron shelving technique described previously in [9, 17] and specifically for this experiment in [9]. Shelving was accomplished by means of a home built 455 nm ECDL. Because of the strength of the transition it was convenient to operate the 455 nm laser multi-mode, which enabled us to drive the shelving transition without active wavelength stabilization. Using this scheme, we were able to reach the shelved state in under 5 ms, which was limited by the speed of that system's mechanical shutter. To remove the ion from the shelved state we used a frequency-doubled 1228 nm beam producing a beam at 614 nm. For the purposes of this experiment the open loop stability of that laser was sufficient that it did not require active frequency stabilization.

The $6S_{1/2} \leftrightarrow 5D_{3/2}$ transitions, which contain the M1 moment of interest, were exited using a diode pumped solid-state (TmHo:YLF) laser operated at 2.051 μm [18]. The laser was stabilized against an ultra-low expansion optical resonator that was measured to have a finesse greater than 350,000 [19, 20]. Because of the availability of optical coatings at the time of its construction, to achieve such a high finesse

cavity it was necessary to stabilize it against the beam's second harmonic at 1.025 μm. Of the 40 mW of 2.051 μm light available, only 3 mW were delivered to the ion for spectroscopy, while the rest was used for stabilization. At the time of writing our best bound on the laser's bandwidth – which was set in the course of this work – was lower than 70 Hz.

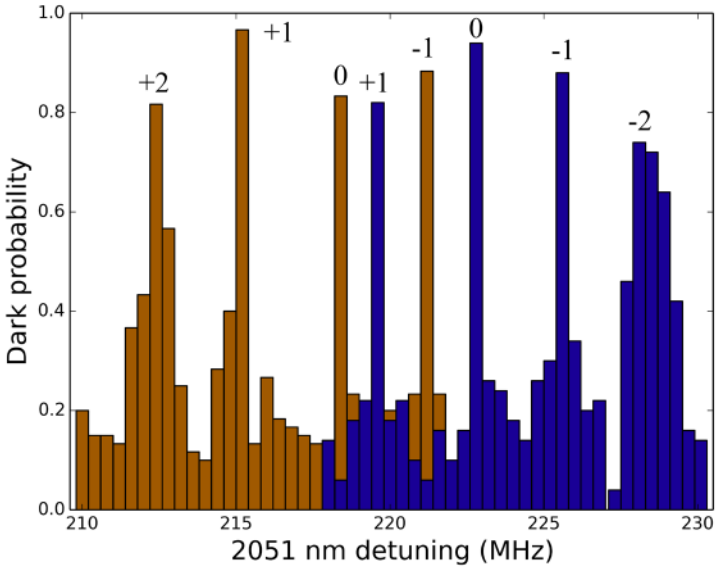

Fig 2. (Color online) Data from two adiabatic rapid pas-sage scans that identify all eight 2.051 μm transitions through the probability of finding the ion in the dark state plotted against our frequency offset to the 2.051 μm beam's nominal frequency. Each bin is 400 kHz wide, corresponding to the width of the ARP sweep. For the orange scan we optically pumped to the $6S(m_j = -1/2)$ state and for the blue to the $6S(m_j = +1/2)$ state. From left to right the tall orange bins correspond to $\Delta m = +2, +1, 0, -1$, the blue to $\Delta m = +1, 0, -1, -2$.

The 2.051 μm transitions were separated by about 3 MHz, and were power broadened to between tens of kilohertz to tens of hertz, depending on the field alignment. To roughly locate the transitions we used adiabatic rapid passage (ARP) [21, 22]. Examples of two ARP scans, corresponding to the atom initially prepared in either of its $6S_{1/2}$ ground states, are shown in Fig 2. Within those scans all eight 2.051 μm transitions are evident, and are labeled by their corresponding change in the magnetic quantum number.

4 Data and Analysis

To obtain all of the necessary pieces needed to get M1, three measurements were undertaken; first of $\Omega^{(0)}$, then $\Omega^{(+2)}$ alone, then $\Omega^{(\pm 2)}$ measured simultaneously. All Rabi frequency measurements were performed using the electron-shelving technique described in [9]; a sample Rabi oscillation is displayed in Fig (3). The first two Rabi oscillation data sets were used to calculate M1 without correcting for 2.051 μm ellipticity, and the Ω^{+2} data were used to extract the viewport birefringence parameters to account for ellipticity in the beam. In all cases the Rabi frequency measurements were taken at 10° intervals of half-wave plate rotation, except near the minimum of $\Omega^{(0)}$ where more data was needed. The half-wave plate position was set manually using a Thorlabs PRM1 high-precision rotation mount, which had an angular resolution of five arc-minutes read off a vernier scale. All Rabi frequency measurements were recorded with respect to the reading of the half-wave plate's rotation mount which were assigned a ± 10 arc-minute (0.16°) error bar to overestimate error from vernier acuity. The rotation was always carried out from low

angle to high angle to avoid inconsistency from backlash. We did not know a priori how the half-wave plate was oriented in its rotation mount (with respect to the plane spanned by the 2.051 μm $\vec{k}$ vector and the ion's quantization axis), so in all cases the data were fit with an additional phase offset ϕ_0 to account for this initial alignment.

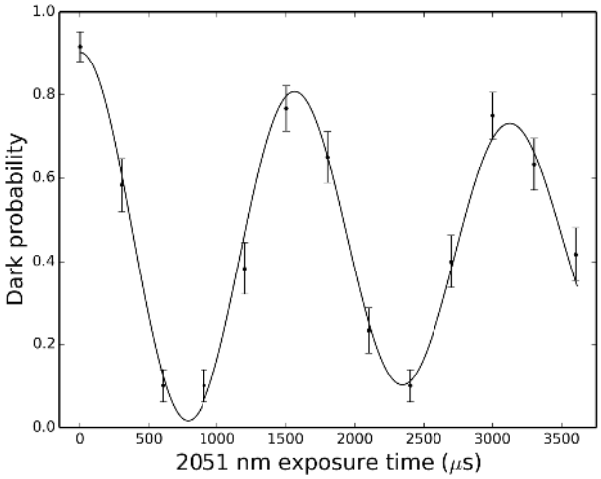

Fig 3. An example of a Rabi oscillation measured for one of the Δm = 0 transition. The probability of finding the ion in the dark state is shown against the 2.051 μm exposure time. For each exposure time the measurement was repeated one hundred times and the data were fit to a theoretical model accounting for the efficiency of shelving [9].

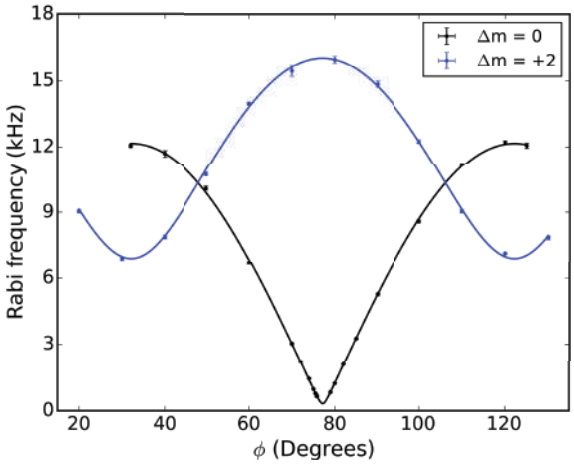

Fig 4. (Color online) Plots of the ç(0) and ç(+2) data sets along with their fits, which are described in the text. The curve in blue is the m = +2 transition and that in black is the m = 0 transition.

The data for $\Omega^{(+2)}(\phi)$ and $\Omega^{(0)}(\phi)$ are plotted together in Fig 4. For the small amounts of ellipticity we encountered, the principle effect of the viewport in the $\Omega^{(0)}(\phi)$ data is to raise the minimum value observed, $\Omega^{(0)}_{min}$ without significantly skewing the location of the minimum. The consequence of these observations is that, to a good approximation, $\Omega^{(0)}$ is,

$$\Omega^{(0)} \approx \sqrt{|\Omega^{(0)}_{mac}|^2 \sin^2(2\phi - 2\phi_0) + |\Omega^{(0)}_{min}|^2 \cos^2(2\phi - 2\phi_0)} \tag{7}$$

The parameter $\Omega^{(0)}_{min}$ includes the M1 coupling plus some E2 coupling due to unintended elliptical polarization that can be subtracted out if the viewport parameters are known. Because uncertainty in $\Omega^{(0)}_{min}$ leads our uncertainty in the value of M1 we will report, we refine our reported uncertainty with an asymmetric estimation in the uncertainty of $\Omega^{(0)}_{min}$. Our methodology for asymmetrically estimating the uncertainty in $\Omega^{(0)}_{min}$ was to refer to χ^2 of $\Omega^{(0)}$ as a function of $\Omega^{(0)}_{min}$. Next, we also require the alignment angle between the 2.051 μm laser and the ion's quantization axis θ, which we get from the stand-alone measurement of $\Omega^{(+2)}$.

Table 1. Fit parameters for the $\Omega^{(0)}(\phi)$ and $\Omega^{(+2)}(\phi)$ measurements

$\Omega^{(0)}$	$\Omega^{(0)}_{max}/2\pi$ (Hz)	$\Omega^{(0)}_{min}/2\pi$ (Hz)	ϕ_0 (Degrees)
	12156 ± 35	319 + 32 − 36	77.18° ± 0.02°
$\Omega^{(+2)}$	C_{E2} (Hz)	θ (Degrees)	ϕ_0 (Degrees)
	17764 ± 81	64.4 + .3	77.16° ± 0.19°

The angle θ is a fit parameter to that data and determines the amplitude of the oscillation observed in $\Omega^{(+2)}(\phi)$. The effect of ellipticity in the beam is to skew the data both vertically and horizontally which shifts 8's apparent value, however that effect contributes minimally to our final M1 value. To obtain θ we approximate the laser fields as linearly polarized, which leads to,

$$\Omega^{(+2)} \approx C_{E2} \sin(\theta) \sqrt{\cos^2(\theta)\sin^2(2\phi - 2\phi_0) + \cos^2(2\phi - 2\phi_0)}, \tag{8}$$

where C_{E2} is $\frac{k/E/E_2}{2\sqrt{30\hbar}}$. Once we have the viewport parameters we can correct θ to get closer to the true value, where we will find about a 1° shift. That withstanding, M1 is not particularly sensitive to θ, at least for our chosen geometry, so this correction is not critical for the experiment's interpretation. An important indicator that our approximations are valid is that the data sets remain well-aligned, indicated by the fitted values of ϕ_0 in agreement to a few hundredths of a degree for the two transitions.

Solving for M1 from Eq (5), and inserting the fit parameters in Table 1, we find that

$$\begin{aligned} \mathrm{M1} &= \sqrt{\frac{3}{5}} \times \frac{ckE2}{2} \times \frac{\Omega^{(0)}_{min}}{\Omega^{(0)}_{max}} \times \cos(\theta) \\ &= 246 \pm 26 \times 10^{-5}\ \mu\mathrm{B}\ (\text{No ellipticity correction}) \end{aligned} \tag{9}$$

To reach this value we have ignored any effects from ellipticity in the laser fields, which was nearly all induced by the ultra-high vacuum viewport. In the following section we will account for ellipticity in the beam by inferring the effective retardance, Γ, and orientation of the optical axis, α, of that viewport with an *in situ* measurement.

5 Calibration of viewport birefringence

Stress in optical windows is well known to induce birefringence which can hinder precision measurements. Several recent papers have addressed the topic with methods for mitigating or measuring the effect [23-25], however for our purposes a new technique was required. When driven with an elliptically polarized field, the minimum in the Δm = 0 transition, $\Omega^{(0)}_{min}$ acquires an additional contribution from electric-quadrupole coupling, $\Omega^{(\varepsilon)}_{min}$, which from Eq (10) is,

$$\Omega^{(0)}_{\min} = \left| \frac{ik}{4\sqrt{10\hbar}} E2 \sin(2\theta) E\| (|E|, \phi_0, \alpha, \Gamma) - \frac{1}{\sqrt{6\hbar}} M1 \sin(\theta) B\| (|E|, \phi_0, \alpha, \Gamma) \right.$$
$$\left. - \frac{1}{\sqrt{6\hbar}} M1 \sin(\theta) B\| (|E|, \phi_0, \alpha, \Gamma) \right| \tag{10}$$
$$= \left| \Omega^{(\varepsilon)}_{\min} + A^{(M1)}_{min} \times M1 \right|$$

and from which M1 can be calculated once the view- port optical axis orientation, α, and its retardance, Γ are known.

To experimentally determine the viewport optical parameters, we measured $\Omega^{(\pm 2)}$ (ϕ) concurrently. For a perfectly linear polarized beam these transition's Rabi frequencies are identical, however, when driven with an elliptically polarized field, interference between the different couplings causes the $\Omega^{\pm 2}$ (ϕ) curves to become skewed with respect to one another. Where the two curves cross over each other indicates the orientation of the optical axes, and their relative skew increases with Γ. The data are plotted in Fig 5, where the blue and red curves are Δm of +2 and –2, respectively.

These data were collected and interpreted in isolation from the previous data sets because of changes that were required of the system for another experiment. However, the 2.051 μm pointing through the viewport was not changed. The data were collected by fixing the beam's polarization and measuring both of the ± 2 transition Rabi frequencies before rotating the beam's polarization.

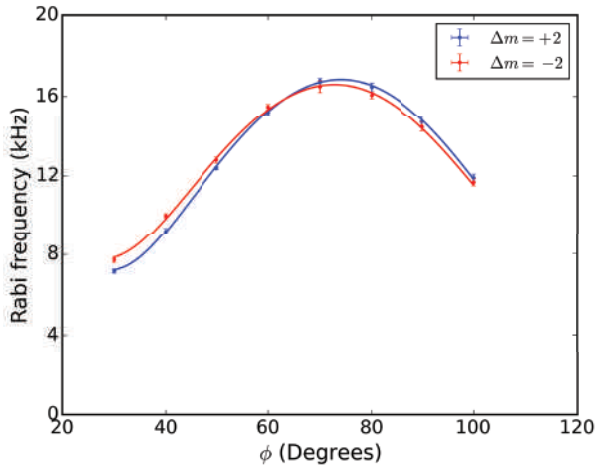

Fig 5. The data and the fit of the $\Omega^{(\pm 2)}$ measurements fitted simultaneously to the birefringence laser field model. The blue indicates the Δm = +2 data and the red indicates the Δm = –2 data.

The precision to which α and Γ are extracted can be greatly improved by taking combinations of the data sets that exaggerate the effect of those parameters by masking the influence of other extraneous parameters. The first of these combinations is the ratio $\Omega^{(+2)}/\Omega^{(-2)}$ which for perfect linear polarized light does not deviate from unity. Because in taking the ratio the electric field amplitude is canceled, to first order any deviation of $\Omega^{(+2)}/\Omega^{(-2)}$ from unity is due to Γ alone. The purpose of measuring both ± 2 Rabi frequencies at a given half-wave plate orientation before moving to the next position was to minimize the possibility that the laser field amplitude could have changed significantly between the scans. To that concern though, over the several years during which this measurement was refined, there was never any indication that such laser field changed meaningfully over the course of an experiment. The second combination of

the data is the squared difference between the two data sets, $|\Omega^{(+2)}|^2 - |\Omega^{(-2)}|^2$, which simplifies to,

$$|\Omega^{(+2)}|^2 - |\Omega^{(-2)}|^2 = 2A \sin[4(\phi - \phi_0) - 2\alpha] \tag{11}$$

The coefficient $A = k/(4\sqrt{10\hbar})|E|E2\sin(2\theta)\cos(\theta)\sin(\Gamma)$, and does not provide information about those parameters, but the combination is useful for obtaining α. To do this we use the known value of ϕ_0 which leaves α as a second free parameter of the model. From these two combinations of the data we obtain the viewport parameters that are given in the table in Fig 6, and additionally with the parameters in Table 1, we find,

$$\mathrm{M1} = 93 + 38 - 40 \times 10^{-5}\ \mu\mathrm{B}\ \text{(with ellipticity correction)} \tag{12}$$

Our reported uncertainty is from the quadrature sum of those from $\Omega^{(0)}_{min}$, $\Omega^{(\varepsilon)}_{min}$, and $\Omega^{(\mathrm{M1})}_{min}$, Table 2 summarizes the error propagation. The uncertainty from measuring $\Omega^{(0)}_{min}$ is the largest single contributor, with that from $\Omega^{(\varepsilon)}_{min}$ contributing an almost equal portion. In the latter, as well as in $\mathrm{A}^{(\mathrm{M1})}_{min}$, the uncertainty in the calculated fields dominate, which are themselves dominated by the uncertainty in Γ.

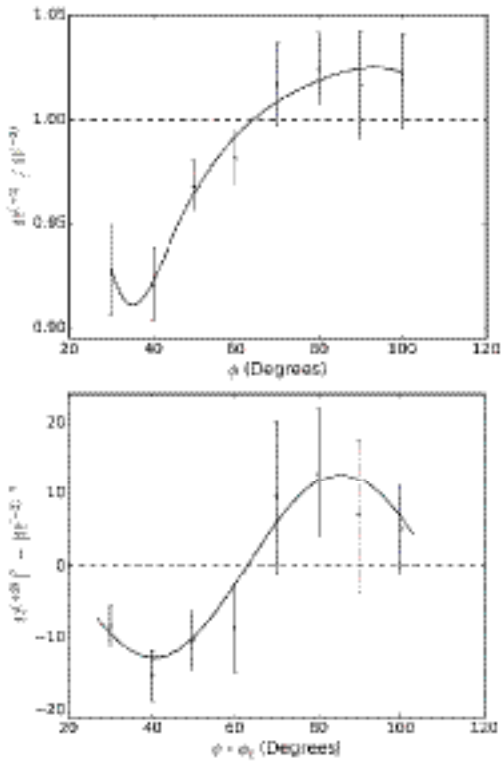

$\Omega^{(+2)}/\Omega^{(-2)}$	Γ(Degrees)	α (Degrees)
	2.8° ± 0.3°	155° ± 9°
$\lvert\Omega^{(+2)}\rvert^2 - \lvert\Omega^{(-2)}\rvert^2$	A (Hz^2)	α (Degrees)
	3.57° ± 07°	159° ± 1.6°

Fig 6. The top panel shows a plot of the ratio between the $\Omega^{(+2)}$ and $\Omega^{(-2)}$ data sets and the bottom panel shows a plot of the square difference $|\Omega^{(+2)}|^2 - |\Omega^{(-2)}|^2$. From these curves we are able to extract the viewport optical axis orientation and retardance experienced by the 2.051 μm beam, which are listed in the table.

Table 2. A summary of the propagated uncertainty to M1. The parameters defined in Eq (10) are demarked by *Y*. The largest fractional contributors to their uncertainty are given in the *X* column. The relative uncertainty in E2 is estimated from [12] to be 1%. The uncertainty in $|E_{||}|$ and $|B_{||}|$ were obtained by propagating the uncertainties from $|E|$, ϕ_0, α, and Γ.

Y/2π	*X*	$\lvert\partial Y / \partial X\rvert$	σ_x / Y	$\lvert\partial \mathrm{M1} / \partial Y\rvert$	σ_Y
$\Omega^{(0)}_{min}$	– –	– –	– –	$+26 \times 10^{-5}\ \mu_B$	
				$-29 \times 10^{-5}\ \mu_B$	
$\Omega^{(\varepsilon)}_{min}$					
	$\lvert E_{\|\|}\rvert$	0.148			
	E_2	0.010			
	θ	0.005		$24 \times 10^{-5}\ \mu_B$	
$\Omega^{(\mathrm{M1})}_{min}$					
	$\lvert B_{\|\|}\rvert$	0.029			
	θ	0.003			
				$13 \times 10^{-5}\ \mu_B$	
		Total σ_{M1}		$+38 \times 10^{-5}\ \mu_B$	
				$-40 \times 10^{-5}\ \mu_B$	

6 Conclusions

By performing a polarization-based spectroscopy of the $6S^{1/2} \leftrightarrow 5D_{3/2}$ transitions in Ba^+, we made the first measurement of the magnetic dipole transition moment connection those states. In the course of doing so we have also demonstrated how our technique can be used to measure stress-induced birefringence in ultra-high vacuum view ports. Several pathways for improvement exist for a next iteration of this experiment. To improve the ability to resolve $\Omega^{(0)}_{min}$ efforts are underway to reduce our measurement's decoherence rate, which was in majority set by ambient magnetic field noise. This could be mitigated with the implementation of magnetic shielding. A complementary strategy would be to enlarge $\Omega^{(0)}_{min}$ by delivering more 2 μm light to the ion. Also, as our measurement has shown, ellipticity can be leveraged – if sufficiently well calibrated – to enhance the size of $\Omega^{(0)}_{min}$. This approach could be improved by eliminating stress-birefringence from the system and introducing a large but known amount of ellipticity separately. This reasoning leads naturally to a version of our measurement using a circularly polarized 2 μm laser field, which we have proposed in [9] and [26].

Acknowledgements

The authors thank the other members of the University of Washington's Trapped Ion Quantum Computing group for their varied and valuable assistance through-out, and also to Matt Dietrich of Argonne National Laboratory for his valuable insights. We also thank the National Science Foundation for their generous support during the early stages of this work.

References

1. Fortson Norval, Possibility of measuring parity nonconservation with a single trapped atomic ion, *Phys Rev Lett,* 70(1983)2383; doi: 10.1103/PhysRevLett.70.2383.
2. Marciano William J, Rosner Jonathan L. Atomic parity violation as a probe of new physics, *Phys Rev Lett,* 65(1990)2963-2966; doi:10.1103/PhysRevLett.65.2963.

3. Fortson E N, Pang Y, Wilets L, Nuclear-structure effects in atomic parity nonconservation, *Phys Rev Lett,* 65(1990)2857-2860; doi: 10.1103/*Phys. Rev. Lett.* 65.2857.
4. Pollock S J, Fortson E N, Wilets L, Atomic parity nonconservation: Electroweak parameters and nuclear structure, *Phys Rev* C, 46(1992)2587-2600; doi:10.1103/PhysRevC.46.2587.
5. Flambaum V V, Khriplovich I B, Sushkov O P, Nuclear anapole moments, *Phys Lett B*, 146(1984)367-369; doi: doi.org/10.1016/0370-2693(84)90140-0.
6. Gwinner G, Gomez E, Orozco L A, Gaivan A Perez, Sheng D, Zhao Y, Sprouse G D, Behr J A, Jackson K P, Pearson M R, Aubin S, Flambaum V V, TCP 2006: Proceedings of the 4th International Conference on Trapped Charged Particles and Fundamental Physics (TCP 2006) held in Parksville, Canada, 3-8 September, 2006, Chapter Fundamental symmetries studies with cold trapped francium atoms at ISAC, pp 45-51. Springer Berlin Heidelberg, Berlin, Heidelberg, 2007. ISBN 978- 3-540-73466-6; doi:10.1007/978-3-540-73466-6_7.
7. DeMille D, Cahn S B, Murphree D, Rahmlow D A, Kozlov M G, Using molecules to measure nuclear spin-dependent parity violation, *Phys Rev Lett*, 100(2008)023003; doi: 10.1103/PhysRevLett.100.023003.
8. Tsigutkin K, Dounas-Frazer D, Family A, Stalnaker J E, Yashchuk V V, Budker D, Parity violation in atomic ytterbium: *Experimental sensitivity and systematics*, *Phys Rev* A, 81(2010)032114; doi: 10.1103/PhysRevA.81.032114.
9. Williams Spencer R, Jayakumar Anupriya, Homan Matthew R, Blinov Boris B, Fortson E N, Method for measuring the $6S_{1/2} \leftrightarrow 5D_{3/2}$ magnetic-dipole-transition moment in Ba^+, *Phys Rev* A, 88(2013)012515 ; doi: 10.1103/PhysRevA.88.012515.
10. Roberts B M, Stadnik Y V, Dzuba V A, Flambaum V V, Leefer N, Budker D, Parity-violating interactions of cosmic fields with atoms, molecules, and nuclei: Concepts and calculations for laboratory searches and extracting limits, *Phys Rev* D, 90(2014)096005; doi:10.1103/PhysRevD.90.096005.
11. Choi J, Elliott D S, Measurement scheme and analysis for weak ground-state-hyperne-transition moments through two-pathway coherent control, *Phys Rev* A, 93(2016)023432; doi:10.1103/ *PhysRev* A.93.023432.
12. Sahoo B K, Islam Md R, Das B P, Chaudhuri R K, Mukherjee D, Lifetimes of the metastable $2d_{3/2;5/2}$ states in Ca^+, Sr^+, and Ba^+, *Phys Rev* A, 74(2006)062504; doi:10.1103/PhysRevA.74.062504.
13. Yu N, Nagourney W, Dehmelt H, Radiative lifetime measurement of the Ba^+ metastable $d_{3/2}$ state, *Phys Rev Lett*, 78(1997)4898-4901; doi: 10.1103/PhysRevLett.78.4898.
14. Gossel G H, Dzuba V A, Flambaum V V. Calculation of strongly forbidden M1 transitions and g-factor anomalies in atoms considered for parity-nonconservation measurements, *Phys Rev* A, 88(2013)034501; doi: 10.1103/*Phys. Rev.*A.88.034501.
15. Safronova M S. Private communication, 2014.
16. Steele A V, Churchill L R, Grin P F, Chapman M S. Photoionization and photoelectric loading of barium ion traps. *Phys Rev* A, 75(2007)053404; doi:10.1103/PhysRevA.75.053404.
17. Nagourney Warren, Sandberg Jon, Dehmelt Hans, Shelved optical electron amplifier: Observation of quantum jumps, *Phys Rev Lett,* 56(1986)2797-2799; doi:10.1103/*Phys. Rev. Lett.*56.2797.
18. Kleczewski A, Homan M R, Magnuson E, Blinov B B, Fortson E N, Frequency doubling and stabilization of a Tm,Ho:YLF laser at 2051 nm to a high finesse optical cavity. 2011. URL http://arxiv.org/abs/1105.4400.
19. Notcutt Mark, Ma Long-Sheng, Ye Jun, Hall John L, Simple and compact 1-Hz laser system via an improved mounting configuration of a reference cavity, *Opt Lett*, 30(2005)1815-1817; doi:10.1364/OL.30.001815.
20. Kleczewski Adam. Towards a measurement of the nuclear magnetic octupole moment in barium-137, *Ph D Thesis*, University of Washington, 2011.
21. Grischkowsky D, Coherent excitation, incoherent excitation, and adiabatic states, *Phys Rev A*, 14(1976)802-812; doi:10.1103/PhysRevA.14.802.
22. Noel T, Dietrich M R, Kurz N, Shu G, Wright J, Blinov B B, Adiabatic passage in the presence of noise, *Phys Rev* A, 85(2012)023401; doi: 10.1103/PhysRevA.85.023401.

23. Brakhane Stefan, Alt Wolfgang, Meschede Dieter, Robens Carsten, Moon Geol, Alberti Andrea, Note: Ultra-low birefringence dodecagonal vacuum glass cell, *Rev Sci Inst*, 86(2015)126108; doi: org/10.1063/1.4938281.
24. Solmeyer Neal, Zhu Kunyan, Weiss David S, Note: Mounting ultra-high vacuum windows with low stress-induced birefringence, *Rev Sci Inst*, 82(2011)066105; doi: org/10.1063/1.3606437.
25. Steffen Andreas, Alt Wolfgang, Genske Maximilian, Meschede Dieter, Robens Carsten, AlbertiAndrea, Note: In situ measurement of vacuum window birefringence by atomic spectroscopy, *Rev Sci Inst*, 84(2013)126103; doi:org/10.1063/1.4847075.
26. Williams Spencer, New Techniques and First Results Toward Measuring the $6S_{1/2}$ to $5D_{3/2}$ Magnetic-Dipole Transition Moment in Ba^+. *Ph D thesis, University of Washington,* 2015.

[*Received*: 12.13.2016]